

PAPER

Comparison of experimental and theoretical fully differential cross sections for single ionization of the $2s$ and $2p$ states of Li by Li^{2+} ions

To cite this article: Ebrahim Ghanbari-Adivi *et al* 2017 *J. Phys. B: At. Mol. Opt. Phys.* **50** 215202

View the [article online](#) for updates and enhancements.

Related content

- [Fully differential cross sections for \$\text{Li}^{2+}\$ -impact ionization of \$\text{Li}\(2s\)\$ and \$\text{Li}\(2p\)\$](#)
Omid Ghorbani, Ebrahim Ghanbari-Adivi and Marcelo Fabian Ciappina
- [Fully differential cross sections for \$\text{C}^{6+}\$ single ionization of helium](#)
M Foster, D H Madison, J L Peacher *et al.*
- [Experimental fully differential cross sections for ion-atom impact ionization](#)
D Madison, M Schulz, S Jones *et al.*

Recent citations

- [Fully differential cross sections for \$\text{Li}^{2+}\$ -impact ionization of \$\text{Li}\(2s\)\$ and \$\text{Li}\(2p\)\$](#)
Omid Ghorbani *et al*
- [Large discrepancies observed in theoretical studies of ion-impact ionization of the atomic targets at large momentum transfer](#)
Omid Ghorbani and Ebrahim Ghanbari-Adivi

Comparison of experimental and theoretical fully differential cross sections for single ionization of the $2s$ and $2p$ states of Li by Li^{2+} ions

Ebrahim Ghanbari-Adivi^{1,2} , Daniel Fischer^{1,3} , Natalia Ferreira³, Johannes Goullon³, Renate Hubele³, Aaron LaForge³, Michael Schulz¹ and Don Madison¹

¹ Physics Department and LAMOR, Missouri University of Science and Technology, Rolla, MO, United States of America

² Department of Physics, Faculty of Sciences, University of Isfahan, Isfahan 81746-73441, Iran

³ Max Planck Institute for Nuclear Physics, Saupfercheckweg 1, D-69117 Heidelberg, Germany

E-mail: ghanbari@phys.ui.ac.ir

Received 6 May 2017, revised 19 September 2017

Accepted for publication 20 September 2017

Published 23 October 2017



CrossMark

Abstract

This paper presents experimental measurements of the fully differential cross section for 16 MeV Li^{2+} single ionization of $2s$ ground and the $2p$ excited state of Li in the azimuthal plane. Data were obtained for three different ejected electron energies and two different projectile momentum transfers. The experimental results are compared with theoretical three-body continuum distorted wave-Eikonal initial state calculations and reasonable good agreement is found between theory and experiment. Theory predicts a double peak structure for one of the measured cases and the physical effects producing the double peak are investigated by performing calculations with different interactions either turned on or off.

Keywords: fully differential cross section, ionization, binary peak, recoil peak

(Some figures may appear in colour only in the online journal)

1. Introduction

Single target ionization is, along with single capture and excitation, one of the three basic inelastic reaction channels in collisions of charged particles with atoms. For ionization, in contrast to the other two channels, the final state involves three unbound particles. Consequently, ionization is particularly suitable to study the few-body problem (FBP) [1, 2]. The essence of the FBP is that, so far, no analytic solution for the Schrödinger equation has been found for more than two mutually interacting particles and, especially for dynamic systems like collisions, this dilemma represents an enormous challenge to theory. In the case of electron impact, the theoretical description of the few-body dynamics has been extensively tested by measured fully differential cross sections (FDCSs) (for a review see [3]) extracted from

kinematically complete experiments, i.e. experiments which determine the complete momentum vectors of all collision fragments [4, 5]. These studies triggered extensive theoretical efforts and for simple target atoms (H and He), satisfactory agreement between experiment and theory has now been achieved (e.g. [6–8]).

For ion impact, kinematically complete experiments are much more challenging because the much larger projectile mass results in very small (for fast and/or heavy projectiles immeasurably small) scattering angles and changes of magnitude of the projectile momenta. Therefore, the first kinematically complete experiment on ionization by ion impact was only reported more than 30 years after the corresponding experiment for electron impact [9]. The difficulties associated with the large projectile mass were circumvented by measuring the momentum vectors of the recoiling target ion and

the ejected electron, using so-called reaction microscopes (ReMi) or COLTRIMS [10, 11]. The scattered projectile momentum can then be deduced from the kinematic conservation laws. Since then, a large body of measured fully differential data has been generated using this method [12–16] (for a recent review see [17]). For intermediate energy proton impact, experimental FDCS were also obtained by measuring the scattered projectile momentum directly along with the recoil-ion momentum [18–22].

The comparison between experimental and theoretical FDCS for ion impact revealed that here the description of the few-body dynamics is even more challenging than for electron impact. Nevertheless, valuable information between the differences in the few-body dynamics for electron- and ion-impact could be obtained. For example, the presence of the capture channel in the case of ion impact was demonstrated to have a large qualitative effect on the FDCS for ionization for certain kinematic conditions [19]. Furthermore, it was shown that the FDCS can sensitively depend on the projectile coherence length [21–24], which tends to be larger for ion impact by about three orders of magnitude compared to electron impact. Finally, for ion impact, FDCS were measured for much larger perturbation parameters η (projectile charge to speed ratio) [12] which are not accessible for electron impact since the minimal speed corresponding to the ionization threshold cannot be compensated by a large charge state.

One disadvantage of conventional ReMIs is that it is limited to targets which under normal conditions are gaseous. Furthermore, the achievable momentum resolution gets worse with increasing target mass so that in practice FDCS measurements using ReMi are only feasible for light targets. Until recently, experimental FDCS for ionization by ion impact were available only for He and H₂ targets. This has changed with the successful implementation of MOTReMi a few years ago [25, 26]. In this method, the supersonic jet used for the target in conventional ReMIs is replaced by a magneto-optical trap (MOT), where a target temperature of a fraction of a mK is reached through laser-cooling. With this method not only is the achievable recoil-ion momentum resolution significantly improved, but the available target species is extended to just about any atom that can be optically pumped.

So far, FDCSs for single ionization measured using MOTReMi were only reported for one collision system, namely 16 MeV O⁸⁺ + Li [15]. This corresponds to a large perturbation parameter $\eta = 1.3$. Data for FDCS in the perturbative regime and targets other than H₂ and He were not reported yet. Here, we present experimental and theoretical FDCS for 16 MeV Li²⁺ + Li collisions, corresponding to $\eta = 0.2$. Results are obtained for ionization from the 2s state of Li and from the 2p state excited from the ground state by the cooling laser.

2. Experiment

The experiment was performed with the MOTReMi [25, 26] in the test storage ring TSR at the Max Planck Institute for

Nuclear Physics in Heidelberg. The Li²⁺ ions were accelerated to an energy of 16 MeV, injected into the storage ring, and bunched to pulses with a width of a few nanoseconds and a repetition rate of about 3 MHz.

In the MOTReMi, the lithium target atoms were prepared and cooled in a MOT. After ionization of a target atom, the emitted electron and the recoiling Li⁺ ion were detected and momentum analyzed in coincidence. In order to allow simultaneously for the efficient trapping of the atoms as well as for the high-resolution momentum analysis of the electrons, the magnetic field in the target region was switched periodically alternating between trapping and measuring periods (details can be found in [26]). In the measuring period (about 1200 μ s), a homogeneous magnetic field of 11 Gauss was employed parallel to the projectile beam axis. During the trapping period (several milliseconds duration), the homogeneous field was superimposed with a quadrupole magnetic field, which—due the interaction with the cooling laser beams and the Zeeman splitting of the atomic levels in the target atoms—resulted in a position dependent force confining the atoms in the center of the spectrometer.

During the measuring period, the cooling lasers were switched off for a short time (200 μ s), resulting in a population of 100% of the target ground state configuration 1s²2s¹. For the remaining time, the cooling lasers were switched on maintaining a population of about 20% of the atoms in the excited 1s²2p¹ configuration. Because of a slight red-detuning of the laser light from the resonance energy, the energetically lowest Zeeman level was predominantly populated. Therefore, about 85% of the excited atoms had an orbital angular momentum oriented anti-parallel to the magnetic field axis [15, 26].

The cross sections for the ionization from the excited 2p-state were extracted by the weighted subtraction of the spectra obtained in the measuring period with the laser being switched on and switched off, corresponding to mixed 2p–2s and pure 2s populations, respectively (details can be found in [27]). Although this method worked generally very well, it resulted in very large statistical errors for regions in the final momentum space where the probability of 2s ionization was substantially larger than for 2p ionization. For these regions it was not possible to extract statistically meaningful differential cross sections for 2p ionization.

3. Theory

One of the most successful theoretical approaches for ion–atom collisions is the continuum distorted wave-Eikonal initial state (CDW-EIS) approach introduced by Crothers and co-workers in 1982 [28, 29] and it has been further developed and used by several different groups for almost 40 years [30–42]. The CDW-EIS is a semi-classical approach where the projectile motion is approximated classically. Our approach, which we call the three-body distorted wave-EIS (3DW-EIS) theory is a fully quantum mechanical approach. The 3DW-EIS method has been outlined in detail in the literature and applied previously to treat other ion–atom and

ion–molecule collision systems (see e.g. [43] and references therein). However, in order to keep the present discussion self-contained, a short review of this theory is presented. We consider a three-body collision system in which a projectile ion P of charge Z_P , mass M_P and momentum vector \mathbf{K}_i impinges on a neutral target. The collision causes the projectile to be scattered with final momentum \mathbf{K}_f and the ejection of the active electron e with wave vector \mathbf{k}_e . The target T of mass M_T includes a nucleus of charge Z_T and possibly a number of passive electrons which are assumed frozen in their initial states during the collision (i.e. the nucleus together with the passive electrons are treated as a single particle). The influence of these passive electrons on the ionization process is taken into account through an effective potential. Here, we assume $M_P \gg m_e$ and $M_T \gg m_e$, where m_e is the mass of the electron.

The exact transition matrix for the specified reaction, given by Gell-Mann and Goldberger [44] using the two-potential formulation, can be expressed as

$$T_{fi} = \langle \chi_f^{(-)} | W_f^\dagger | \psi_i^{(+)} \rangle + \langle \chi_f^{(-)} | V_i - W_f^\dagger | \beta_i^{(+)} \rangle, \quad (1)$$

where $\psi_i^{(+)}$ is the exact initial state of the system which satisfies outgoing boundary conditions, $\beta_i^{(+)}$ is the asymptotic form of this state, $\chi_f^{(-)}$ is an approximate final state wavefunction which satisfies incoming boundary conditions, V_i is the initial channel interaction between P and the target, and W_f is the final-state perturbation. The above T -matrix can be rewritten as

$$T_{fi} = \langle \chi_f^{(-)} | V_i | \beta_i^{(+)} \rangle + \langle \chi_f^{(-)} | W_f^\dagger | \psi_i^{(+)} - \beta_i^{(+)} \rangle, \quad (2)$$

in which the first term is the 3DW transition matrix [45], which accounts for part of the higher-order contributions through the final-state wavefunction. The second term takes into account additional higher-order effects through the final-state perturbation. The asymptotic initial state of the system, $\beta_i^{(+)}$, in coordinate space is given by

$$\beta_i^{(+)}(\mathbf{r}, \mathbf{R}) = (2\pi)^{-3/2} \varphi_i(\mathbf{r}) e^{i\mathbf{K}_i \cdot \mathbf{R}}, \quad (3)$$

where (\mathbf{r}, \mathbf{R}) are Jacobi coordinates and $\varphi_i(\mathbf{r})$ is the initial bound-state wave function for the active electron. Here, we use a numerical Hartree–Fock wave function for $\varphi_i(\mathbf{r})$. The initial state interaction, V_i , contains the interaction with the active electron $-Z_P/|\mathbf{R} - \mathbf{r}|$, the passive electrons and the nucleus. Green and co-workers [46–48] used an analytic fit to a Hartree–Fock potential to approximate the interaction with the passive electrons and combined this with the nuclear charge to defined an effective screened charge for the target ion, $Z_{\text{eff}}(R)$, which varies from unity at large distances to Z_T for small distances. Consequently, the initial channel interaction V_i can be represented by

$$V_i(\mathbf{r}, \mathbf{R}) = \frac{Z_P Z_{\text{eff}}(R)}{R} - \frac{Z_P}{|\mathbf{R} - \mathbf{r}|}. \quad (4)$$

The final channel wave function is approximated as

$$\chi_f^{(-)}(\mathbf{r}, \mathbf{R}) = \varphi_e(\mathbf{r}) C_P^-(\mathbf{K}_f, \mathbf{R}) D_{Pe}(\mathbf{r}, \mathbf{R}), \quad (5)$$

where the continuum distorted wave for the ejected electron in the field of target ion, $\varphi_e(\mathbf{r})$, is a numerical solution of the Schrödinger equation

$$\left[-\frac{1}{2} \nabla_r^2 - U_{\text{ion}}(r) + \frac{1}{2} k_e^2 \right] \varphi_e(\mathbf{r}) = 0, \quad (6)$$

in which $U_{\text{ion}}(r) = -Z_{\text{eff}}(r)/r$ is the static Hartree–Fock potential of the target ion T , $C_P^-(\mathbf{K}_f, \mathbf{R})$ is a Coulomb wave for propagation of P in the field of T and $D_{Pe}(\mathbf{r}, \mathbf{R})$ is a Coulomb distortion factor representing the post-collision interaction between P and e .

The explicit form of the final-state perturbation potential, $W_f(\mathbf{r}, \mathbf{R})$, depends on the choice for the final-state wave function. With the above approximation for $\chi_f^{(-)}(\mathbf{r}, \mathbf{R})$ given in equation (5), this potential can be calculated using the differential equation

$$(H - E) \chi_f^{(-)}(\mathbf{r}, \mathbf{R}) = W_f(\mathbf{r}, \mathbf{R}) \chi_f^{(-)}(\mathbf{r}, \mathbf{R}), \quad (7)$$

in which H is the full Hamiltonian and E is the total energy. In order to have an analytic form for $W_f(\mathbf{r}, \mathbf{R})$, for the calculation of the perturbation we approximate the final state wavefunction for the electron as an analytic Coulomb wave in the form of

$$C_e^-(\mathbf{k}, \mathbf{r}) = (2\pi)^{-3/2} \Gamma(1 - i\gamma) e^{-\frac{\pi\gamma}{2} + i\mathbf{k}_e \cdot \mathbf{r}} \times {}_1F_1[i\gamma; 1; -i(k_e r + \mathbf{k}_e \cdot \mathbf{r})], \quad (8)$$

and use the same perturbation as Crothers and co-workers [28, 29]. In the above Coulomb wave function, $\gamma = 1/v$ where v is the final relative speed of the electron and the residual ion.

In equation (2), if we approximate the exact initial-state wave function, $\psi_i^{(+)}$, as its asymptotic form, $\beta_i^{(+)}$, the second term vanishes and the transition amplitude reduces to the 3DW amplitude. However, it has been found that it is better to approximate this wave function as an EIS [28, 29]. In this approximation, we have

$$\psi_i^{(+)}(\mathbf{r}, \mathbf{R}) \simeq \psi_{\text{EIS}}^{(+)}(\mathbf{r}, \mathbf{R}) = \beta_i^{(+)}(\mathbf{r}, \mathbf{R}) \times \exp \left[i \frac{Z_P}{v_i} \ln \left(\frac{v_i R - \mathbf{v}_i \cdot \mathbf{R}}{v_i |\mathbf{R} - \mathbf{r}| - \mathbf{v}_i \cdot (\mathbf{R} - \mathbf{r})} \right) \right], \quad (9)$$

where \mathbf{v}_i is the projectile velocity in the entrance channel with respect to the target.

Consequently, in the 3DW-EIS approach, the explicit form for the transition amplitude in coordinate space is

$$T_{fi}^{\text{3DW-EIS}} = \int d\mathbf{r} d\mathbf{R} \chi_f^{(-)*}(\mathbf{r}, \mathbf{R}) V_i(\mathbf{r}, \mathbf{R}) \beta_i^{(+)}(\mathbf{r}, \mathbf{R}) + \int d\mathbf{r} d\mathbf{R} \chi_f^{(-)*}(\mathbf{r}, \mathbf{R}) W_f^*(\mathbf{r}, \mathbf{R}) [\psi_{\text{EIS}}^{(+)}(\mathbf{r}, \mathbf{R}) - \beta_i^{(+)}(\mathbf{r}, \mathbf{R})]. \quad (10)$$

Using the expressions given in equations (3)–(5), (7) and (9) for $\beta_i^{(+)}(\mathbf{r}, \mathbf{R})$, $V_i(\mathbf{r}, \mathbf{R})$, $\chi_f^{(-)}(\mathbf{r}, \mathbf{R})$, $W_f(\mathbf{r}, \mathbf{R})$, and $\psi_{\text{EIS}}^{(+)}(\mathbf{r}, \mathbf{R})$, we numerically evaluate the six-dimensional integrals for the transition amplitude using six-dimensional Gauss–Legendre quadrature first suggested and discussed by Jones and Madison [49].

It may be worthwhile to point out the differences between the present theory and the standard continuum (or Coulomb)-distorted-wave-EIS (CDW-EIS) approximation. First, 3DW-EIS is a fully quantum mechanical approach while CDW-EIS is a semi-classical approach using an impact-parameter formulation based on straight-line trajectories for the projectile ion. Second, in the 3DW-EIS both terms in equation (1) are evaluated while the CDW-EIS approach evaluates only the first term. Finally, in the 3DW-EIS numerical Hartree–Fock wave functions are used for the initial bound state for the active electron and numerical distorted waves are used for the final continuum state.

In the center-of-mass frame, the FDCS for a three-body ion-impact ionization process is given by

$$\frac{d^3\sigma}{d\Omega_P d\Omega_e dE_e} = (2\pi)^4 N_e \mu_{Te} \mu_i^2 \frac{K_f k_e}{K_i} |T_{fi}^{3DW-EIS}|^2, \quad (11)$$

where N_e is the number of electrons equivalent to the active electron in the target, $E_e = k_e^2/2$ is the ejected-electron's energy, and the solid angles Ω_P and Ω_e indicate the scattering directions of the projectile and the ionized electron, respectively. The initial reduced mass of the collision system is μ_i , and μ_{Te} is the same for the subsystem ($T + e$).

4. Results

We have measured FDCS for 16 MeV Li^{2+} ionization of the ground state as well as the $2p$ excited state of Li [86% ($m = -1$), 9% ($m = 0$), 5% ($m = +1$)] for three different ejected electron energies ($E_e = 2, 10$ and 20 eV) and two different projectile momentum transfers $\mathbf{q} = \mathbf{K}_i - \mathbf{K}_f$ in a plane perpendicular to the incident beam direction. In the coordinate system we use, the incident beam direction is along the z -axis, the scattering plane is the xz plane, and the projectile is scattered in the $+xz$ plane. As a result, the ejected electron will primarily be emitted in the $-x$ direction and the binary peak will be mostly centered near $-x$. In the plane perpendicular to the beam direction (often called the azimuthal plane), $\phi_e = 0^\circ$ corresponds to the $+x$ axis, $\phi_e = 90^\circ$ corresponds to the $+y$ axis, and $\phi_e = 180^\circ$ corresponds to the $-x$ axis. The largest cross sections would be expected to be near $\phi_e = 180^\circ$. If a three-dimensional plot is made for the cross section, normally there will be a large lobe pointing near the momentum transfer direction and this is generally called the binary lobe and, for our case, the maximum would be near the $-x$ direction. Most of the FDCS measurements made in the past have detected the ejected electron in the scattering plane and the maximum cross section in this plane was called the binary peak. In this measurement, the ejected electrons are detected for a plane cutting through the binary lobe perpendicular to the scattering plane and we will also call the largest cross section in this plane the 'binary peak' as well.

Figures 1 and 2 compare the measurements with the 3DW-EIS results for $2s$ and $2p$ ionization where the experiment has been normalized to theory at the binary peak for each panel. It is seen that overall there is very good agreement between experiment and theory. Theory predicts a double binary peak structure for the $2p$ case 10 eV and $q = 1.0$ a.u.

Although the structure is too sharp to be observable with the present experimental resolution, there is a small indication (one data point) that the structure might be real. No data are shown for the $2p$ case 2 eV and $q = 1.0$ a.u. as well as 20 eV and $q = 0.4$ a.u., since the $2s$ cross sections are too large to be able to get statistically significant results.

The $2s$ cross sections are symmetrical about $\phi_e = 180^\circ$. If both the $m = \pm 1$ sublevels were equally populated, the $2p$ cross sections would also be symmetric about $\phi_e = 180^\circ$. The asymmetry seen in both the experimental and theoretical results stems from the fact that the experimentally prepared target is 86% $m = -1$ (the theoretical calculations were performed using the experimental weights). This has also previously been observed for 16 MeV $\text{O}^{8+} + \text{Li}$ collisions [15]. It is interesting to note that both the experimental and theoretical peaks are to the left of 180° for all measured cases except 10 eV and $q = 0.4$ a.u. where theory predicts no asymmetry and experiment has a small indication of a peak to the right of 180° . On the other hand, theory predicts a significant right shift for 2 eV and $q = 1.0$ a.u. When the $m = -1$ cross section has a peak to the left of 180° , the $m = +1$ cross section has an identical peak shifted the same distance to the right of 180° and vice versa (mirror symmetry) so the sum over all m -values is symmetric. This effect is normally called magnetic dichroism.

Since the data is all collected at the same time, it is possible to cross normalize the experimental cross sections. Figures 3 and 4 show the $2s$ and $2p$ results where experiment is normalized to the 2 eV $q = 0.4$ a.u. binary peak and the other data is cross normalized. Although there is still relatively good agreement between theory and experiment, theory tends to underestimate the size of the binary peak for the other cases increasing q and increasing energy.

4.1. Investigation of the double binary peak

Double binary peaks have been observed in the FDCS for electron-impact ionization of the $2p$ state of neon [50, 51], argon [51–54] and xenon [50] as well as ionization of p-type states of molecules [55], and the present theoretical results suggest that similar types of cross sections might be expected for heavy particle ionization. The very good agreement that was found between the 3DW-EIS and the shape of the experimental data (figures 1 and 2) suggests that the 3DW-EIS approach contains the important physics controlling the shape of the experimental data and this also gives some confidence that the double peak structure may be correct. Consequently, it would be interesting to see what effects cause the double peak to occur.

In the electron-impact ionization experiments in the scattering plane, the double binary peak occurs when the cross section has a minimum in the momentum transfer direction. Whelan [56] suggested that the p -state minimum can be explained using the plane wave impulse approximation (PWIA). In the PWIA, the TDCS is proportional to the square of the momentum space wavefunction. For the binary peak direction, the momentum space wavefunction for p -states is zero and the TDCS is zero. Presumably, the exact zero in the PWIA would turn into a minimum for better

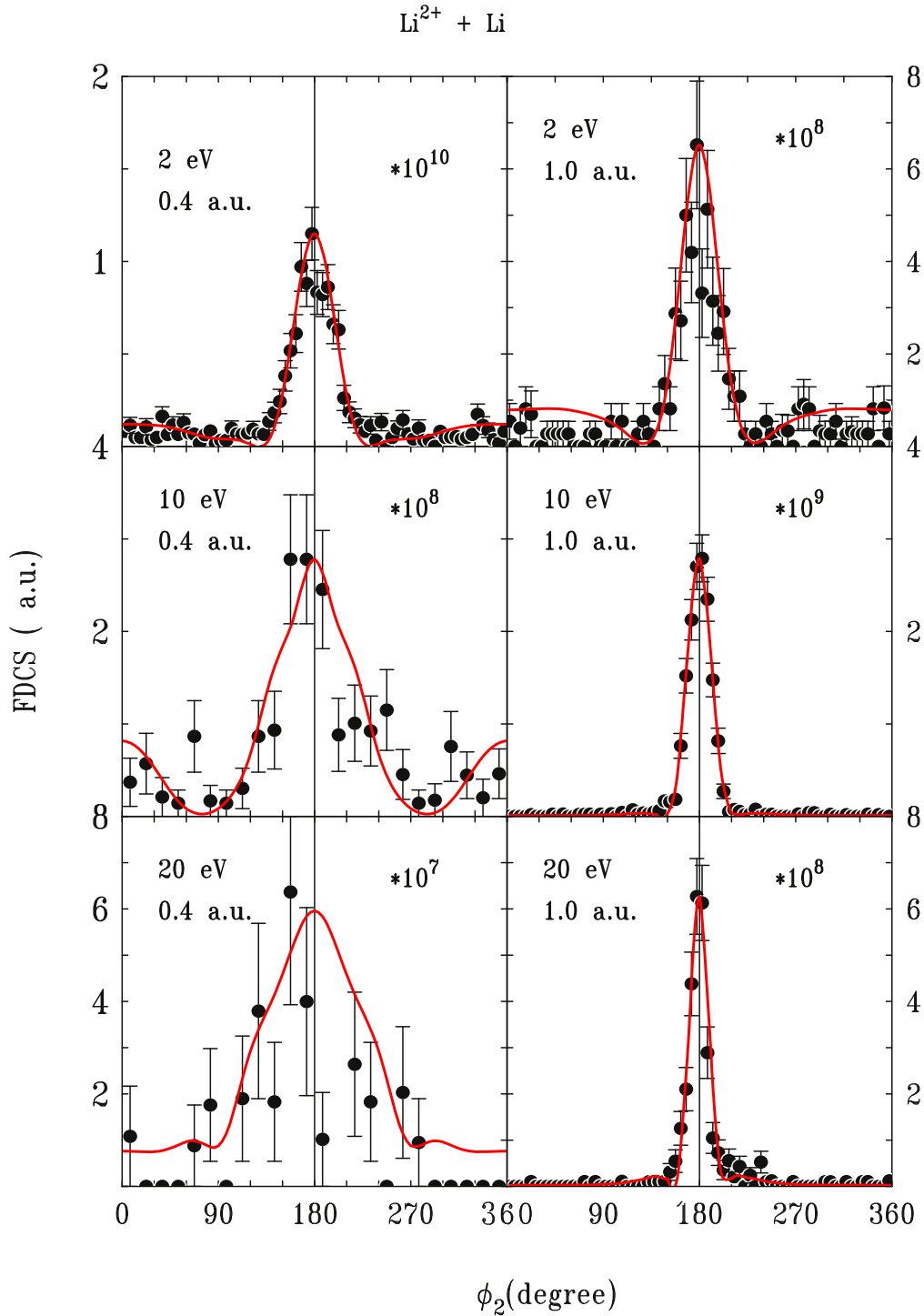


Figure 1. Comparison of experimental and theoretical 3DW-EIS FDSC results for 16 MeV Li^{2+} ionization of the $2s$ shell of Li in the azimuthal plane as a function of the azimuthal angle. The energy of the ejected electron in eV, the momentum transfer of the projectile in atomic units (a.u.), and the magnitude of the cross section in atomic units (a.u.) is noted in each panel. Experiment is normalized to theoretical peaks in each panel.

theoretical approximations. If the three-dimensional binary lobe had a minimum in the direction of the momentum transfer, then there would be a double peak structure both in the scattering plane and in the azimuthal plane.

Since the double peak structure is known to be associated only with ionization of p -states, we first tested to see if the radial part or angular part (or both) caused the double peak.

We first performed a test calculation in which we replaced the $2p$ radial wavefunction with a $2s$ wavefunction while leaving the angular part a p -state and we still found a double binary lobe. Interestingly, the results using the $2s$ radial wavefunction were almost the same as those obtained using the $2p$ radial wavefunction (10%–15% difference in the double peak region). Next, we kept the radial $2p$ wavefunction and

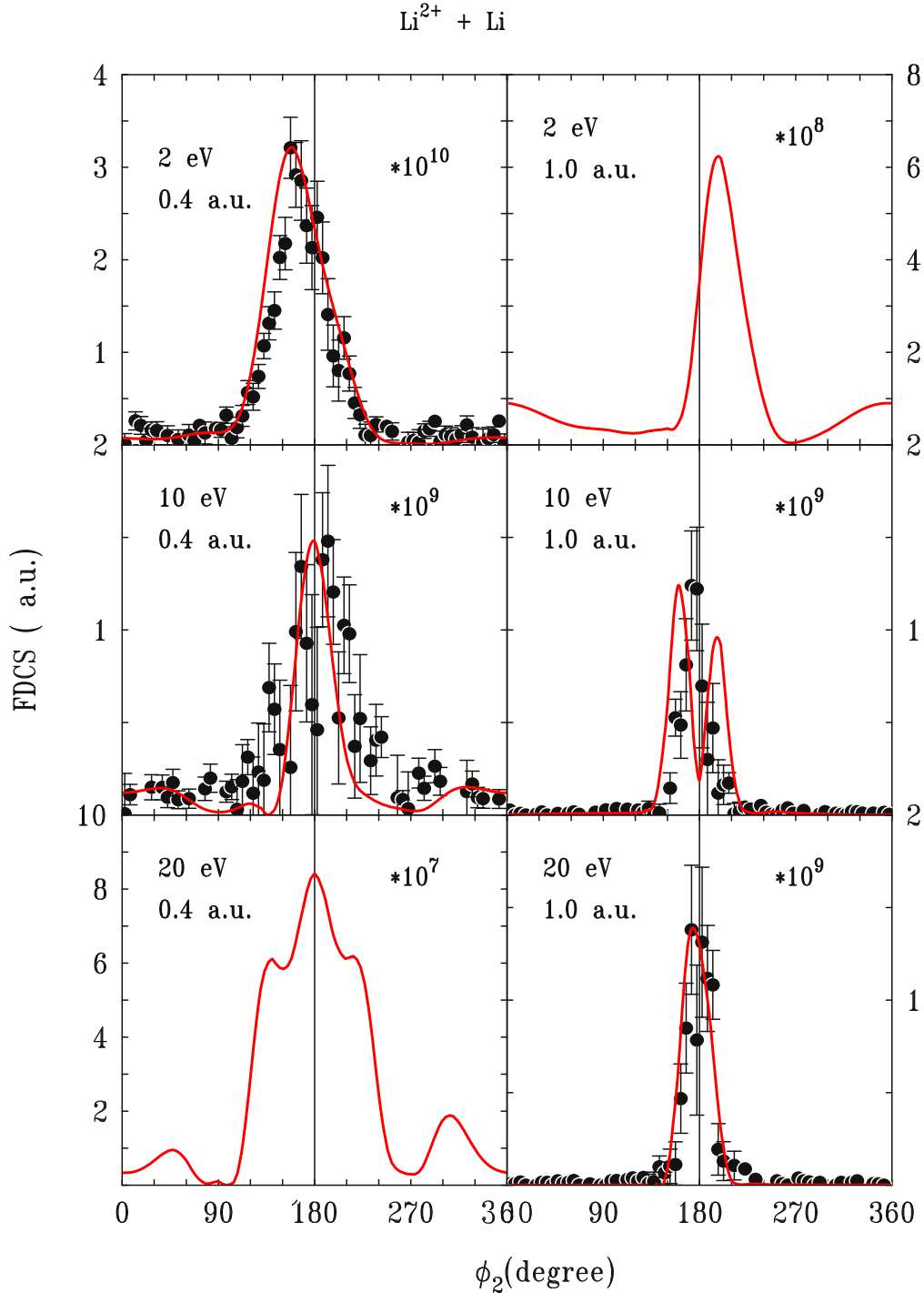


Figure 2. Comparison of experimental and theoretical 3DW-EIS FDCS results for 16 MeV Li^{2+} ionization of the $2p$ shell of Li [86% ($m = -1$), 9% ($m = 0$), 5% ($m = +1$)] in the azimuthal plane as a function of the azimuthal angle. The energy of the ejected electron in eV, the momentum transfer of the projectile in atomic units (a.u.), and the magnitude of the cross section in atomic units (a.u.) is noted in each panel. Experiment is normalized to theoretical peaks in each panel.

replaced the $2p$ angular wavefunction with a $2s$ angular wavefunction. This time the double peak disappeared and the FDCS were symmetric about 180° so the double peak is associated with the angular part of the wavefunction.

For electron-impact ionization, sometimes single peaks have been observed in the p -state FDCS and sometimes double peaks are observed (similar to the present theoretical

predictions) and there has not been a suggestion for a way to predict when to expect a single peak and when to expect a double peak. For 66 eV electron-impact ionization of argon [54], a single binary peak evolved into a double peak for fixed ejected electron energy and increasing projectile scattering angle in one of the three cases measured which is similar to the theoretical prediction presented here.

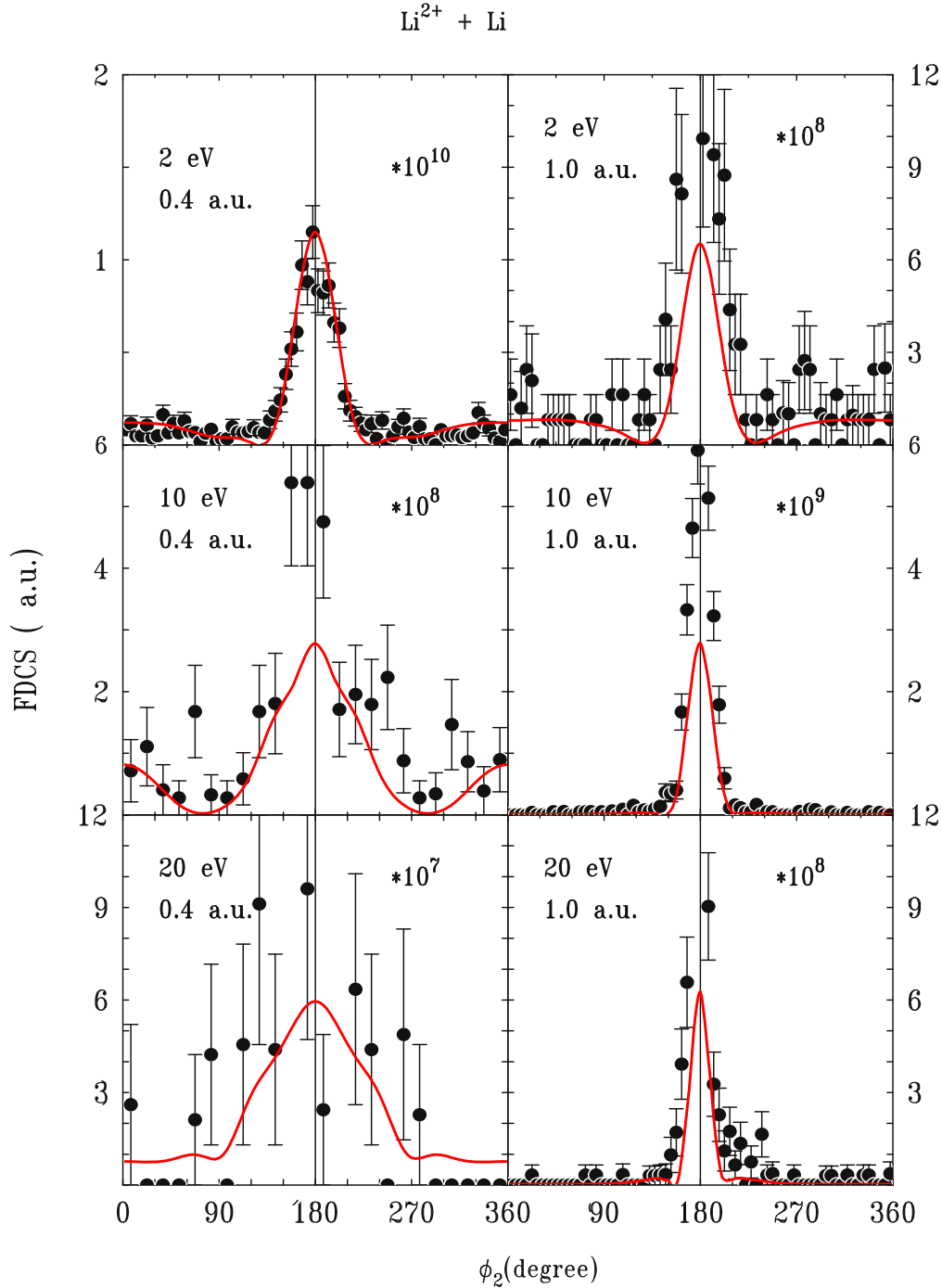


Figure 3. Comparison of experimental and theoretical 3DW-EIS FDCS results for 16 MeV Li^{2+} ionization of the $2s$ shell of Li in the azimuthal plane as a function of the azimuthal angle. The energy of the ejected electron in eV, the momentum transfer of the projectile in atomic units (a.u.), and the magnitude of the cross section in atomic units (a.u.) is noted in each panel. Experiment is normalized to the 2 eV $q = 0.4$ a.u. theoretical peak and the same normalization factor is used for all the data.

To see if we could find a way to predict when a double peak might be expected, we investigated how different interactions within the collision system affected the shape of the cross section. We performed a series of calculations either including or excluding various physical effects. To investigate the importance of the projectile-target ion interaction in the projectile wavefunction, we did a first-Born approximation (FBA) type calculation which contains no projectile-target ion

interaction in the wavefunction. To do this, we set $\psi_i^{(+)} = \beta_i^{(+)}$ and approximated

$$\chi_f^{(-)}(\mathbf{r}, \mathbf{R}) = (2\pi)^{-3/2} \varphi_e(\mathbf{r}) e^{-i\mathbf{K}_f \cdot \mathbf{R}} \quad (12)$$

i.e. we evaluated the first term of equation (2) changing the final state wavefunction for the projectile to a plane wave and left everything else the same. Figure 5 compares experiment with the FBA and 3DW-EIS FDCS results. Surprisingly, for four of the

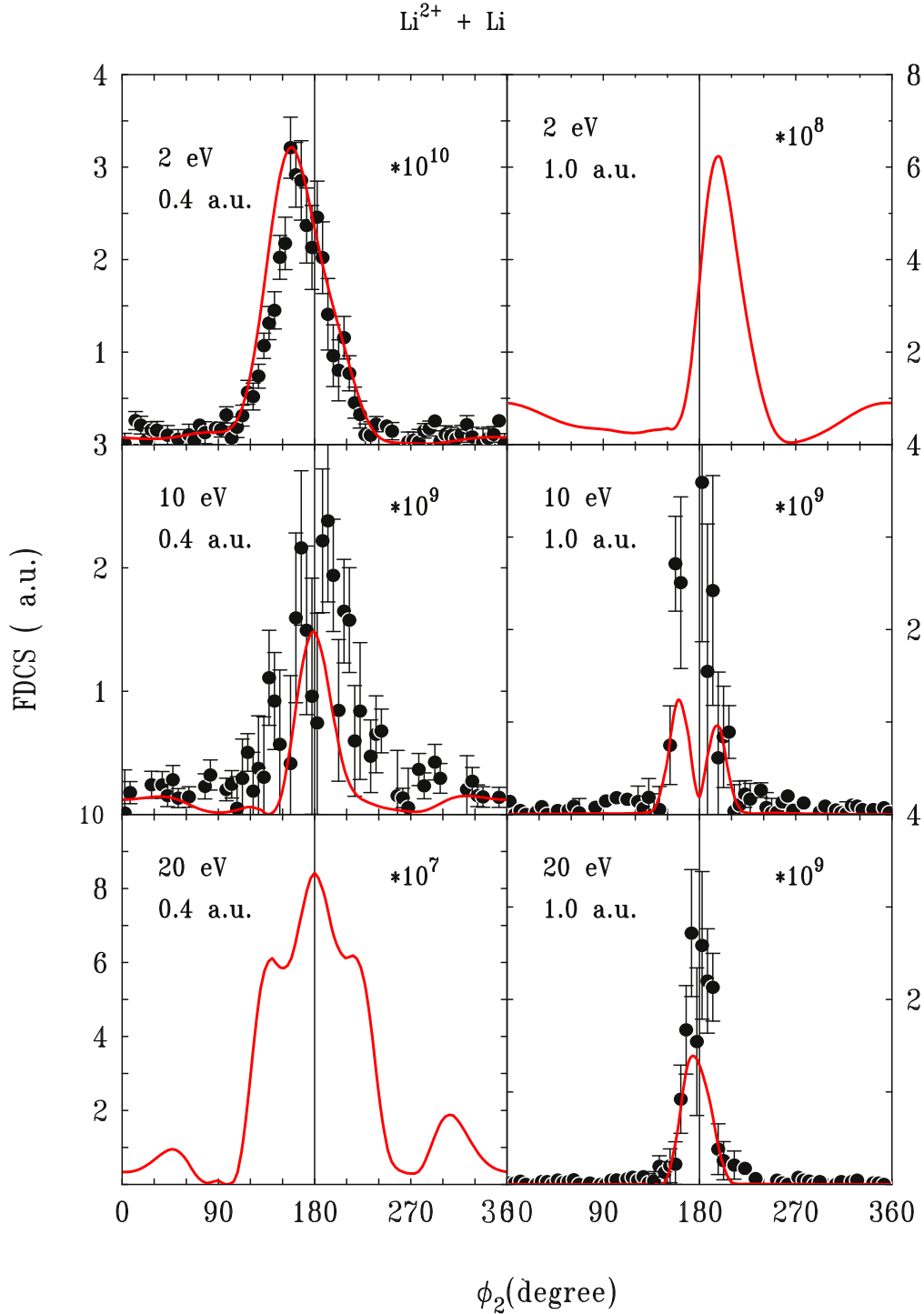


Figure 4. Comparison of experimental and theoretical 3DW-EIS FDCS results for 16 MeV Li^{2+} ionization of the $2p$ shell of Li [86% ($m = -1$), 9% ($m = 0$), 5% ($m = +1$)] in the azimuthal plane as a function of the azimuthal angle. The energy of the ejected electron in eV, the momentum transfer of the projectile in atomic units (a.u.), and the magnitude of the cross section in atomic units (a.u.) is noted in each panel. Experiment is normalized to the 2 eV $q = 0.4$ au theoretical peak and the same normalization factor is used for all the data.

six cases, the results did not change that much and the double binary peak for 10 eV is still predicted. However, for 2 eV and $q = 1.0$ a.u., significant changes in the shape are found and the peak height was reduced by about a factor of 2 in the FBA calculation. For 20 eV and $q = 0.5$ a.u., the two side peaks were eliminated, so the structure seen for this case appears to be caused by the Coulomb interaction between the projectile with

the target ion. However, overall the cross sections are relatively insensitive to the Coulomb interaction in the projectile wavefunction.

Next, we examined the role of ejected-electron-residual target ion interactions in the ejected electron wavefunction $\varphi_e(\mathbf{r})$. In the 3DW-EIS, the ejected electron wavefunction is a numerical solution of equation (6) with $U_{\text{ion}}(r)$ which is a

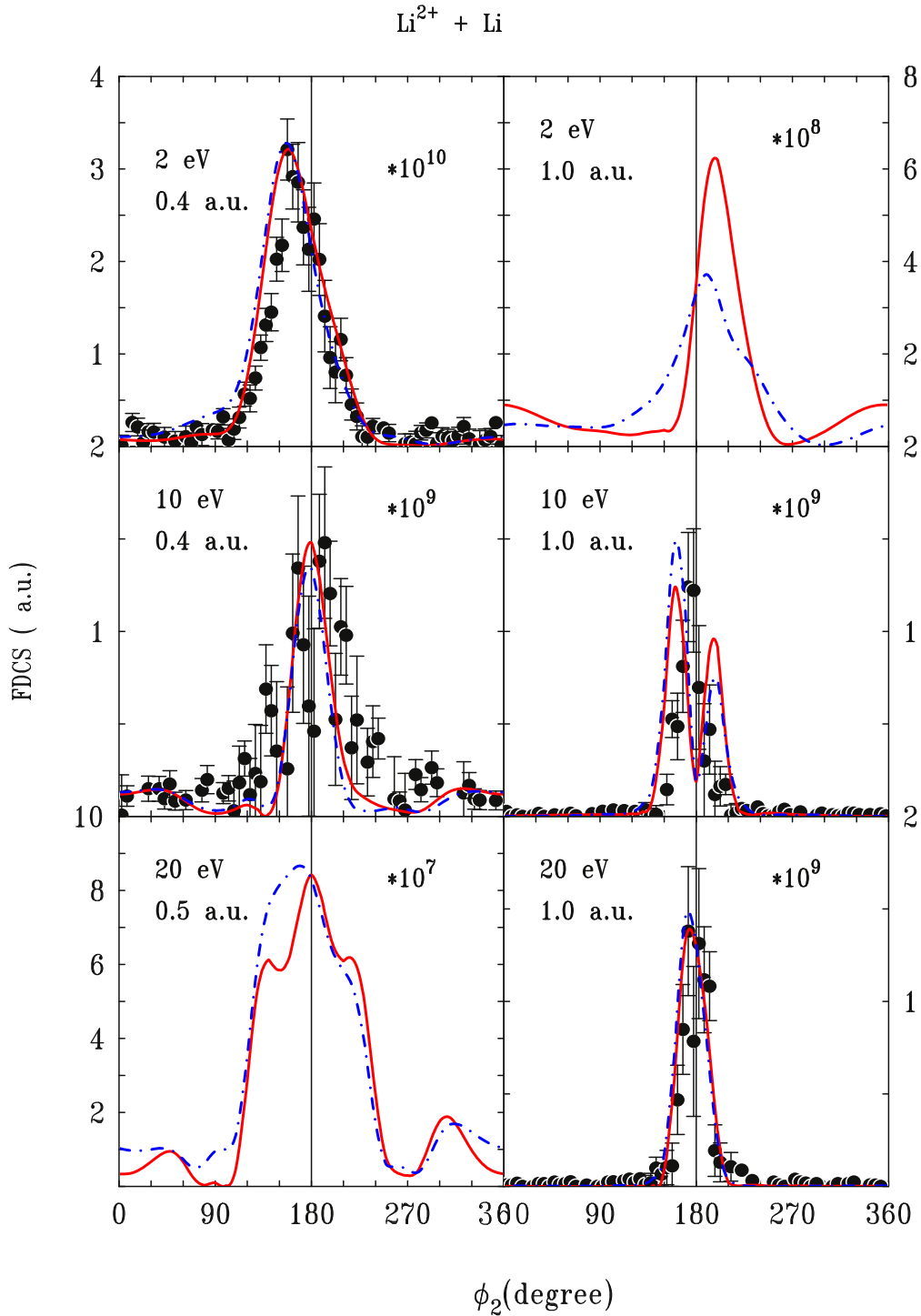


Figure 5. Same as figure 2. Here the solid (red) curves are the 3DW-EIS results and the dot-dashed (blue) curves are the FBA.

potential that is Z_p/r near the origin and $1/r$ asymptotically (normally called a distorted wave). Next we calculated results for the ejected electron being approximated by a Coulomb wave ($U_{\text{ion}}(r) = 1/r$) for all r , as well as results for the ejected electron being approximated as a plane wave ($U_{\text{ion}}(r) = 0$). Everything else was left unchanged in the 3DW-EIS calculation. Figure 6 compares results for the three different ejected electron wavefunctions with experiment. Not surprisingly, the plane wave results were very

different and did not even resemble the experiment for 2 eV. The plane wave results predict double peaks near 180° for both 10 eV and 20 eV for $q = 1.0$ a.u. At first glance it may appear surprising that there is not a larger difference between the Coulomb wave and distorted wave results. With a different normalization, the Coulomb wave results would agree with experiment almost the same as the distorted wave results. The difference between the Coulomb wave and distorted wave occurs for distances close to the nucleus. Apparently,

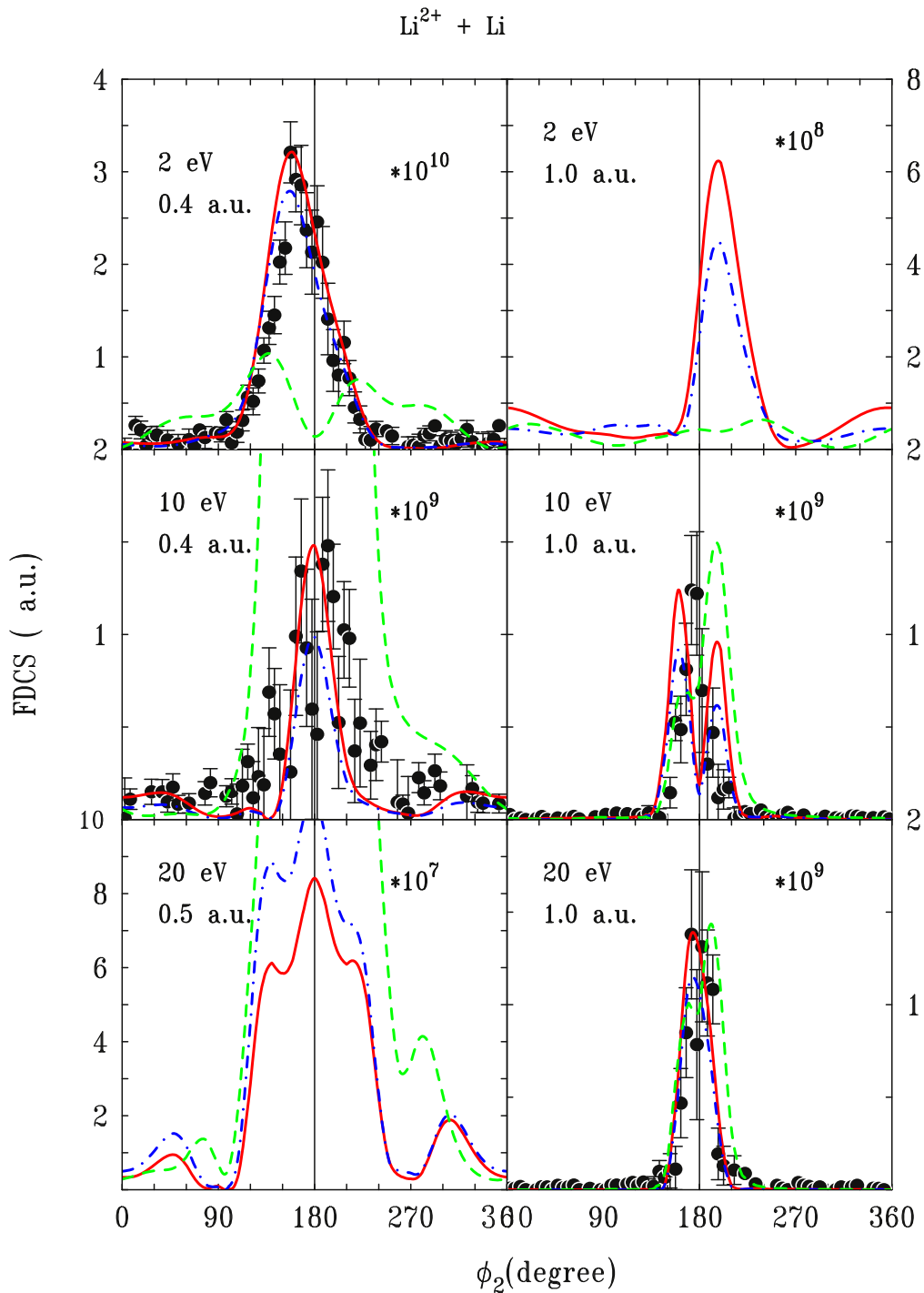


Figure 6. Same as figure 2. The solid (red) curves are the 3DW-EIS results, the dash-dot (blue) curves are 3DW-EIS results with the ejected electron being approximated as a Coulomb wave, and the dashed (green) curves are 3DW-EIS results with the ejected electron being approximated as a plane wave.

the short range behavior of the ejected electron wavefunction is not very important as long as it is at least a Coulomb wave. This can be understood in terms of the very small ionization potential and large (compared to e.g. He) size of the Li atom. Both factors have a tendency of selecting large impact parameters.

For heavy ion collisions, there has been a lot of discussion about the importance on the nucleus–nucleus interaction

[1, 13, 38, 57]. From figure 5, we saw that the projectile–target ion interaction was not particularly important in the projectile wavefunction. The other place it occurs in the calculation is in Z_{eff} in the initial state potential V_i . Consequently, we set $Z_{\text{eff}} = 0$ in V_i and only included the interaction with the active electron. Figure 7 compares 3DW-EIS results with and without the nucleus–nucleus interaction in V_i . It is seen that the two results are almost the same with the biggest change

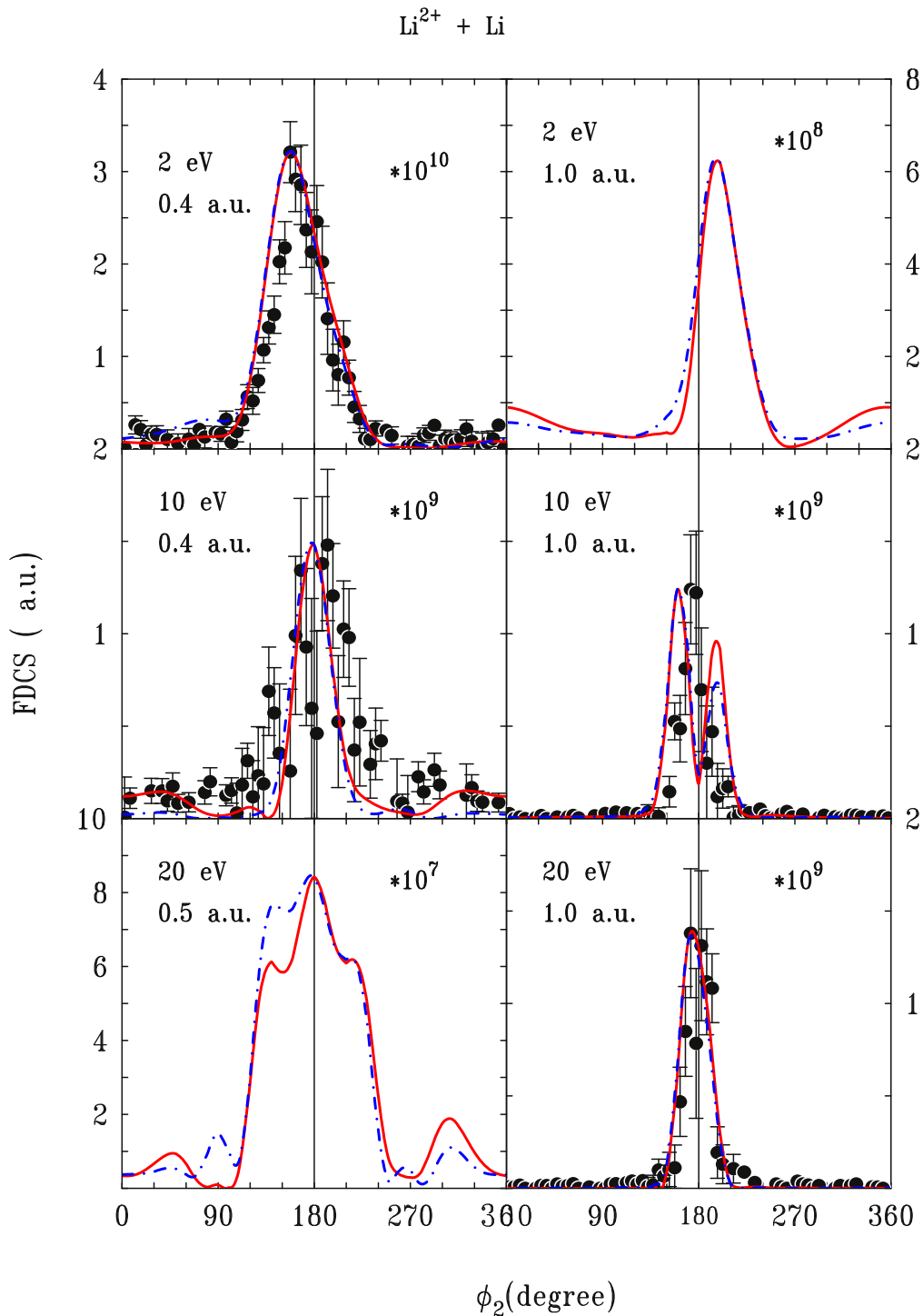


Figure 7. Same as figure 2. The theoretical curves are 3DW-EIS results using different approximations for V_i . The solid curves (red) use the V_i of equation (4). The dash-dot (blue) curves just include the interaction of the projectile with the active electron.

being seen for 20 eV and $q = 0.5$ a.u. It is interesting to note that removing the projectile-target ion interaction from the projectile wavefunction eliminated the side peaks and removing the projectile-target ion interaction from V_i had a noticeable effect only on the low angle side peak which further indicates that the projectile-target ion interaction is responsible for this structure. Otherwise, the projectile-target ion interaction also does not have a very big effect on the

results of the calculation. Apparently, for these kinematics, the only really important aspect is to represent the ejected electron as some form of Coulomb wave.

To further investigate the double peak structure, we performed a series of calculations for 10 eV ejected electrons and different momentum transfer values. The double peak structure started at $q = 0.9$ a.u. and ended at $q = 1.2$ a.u., so it occurs only for a narrow range of momentum transfer.

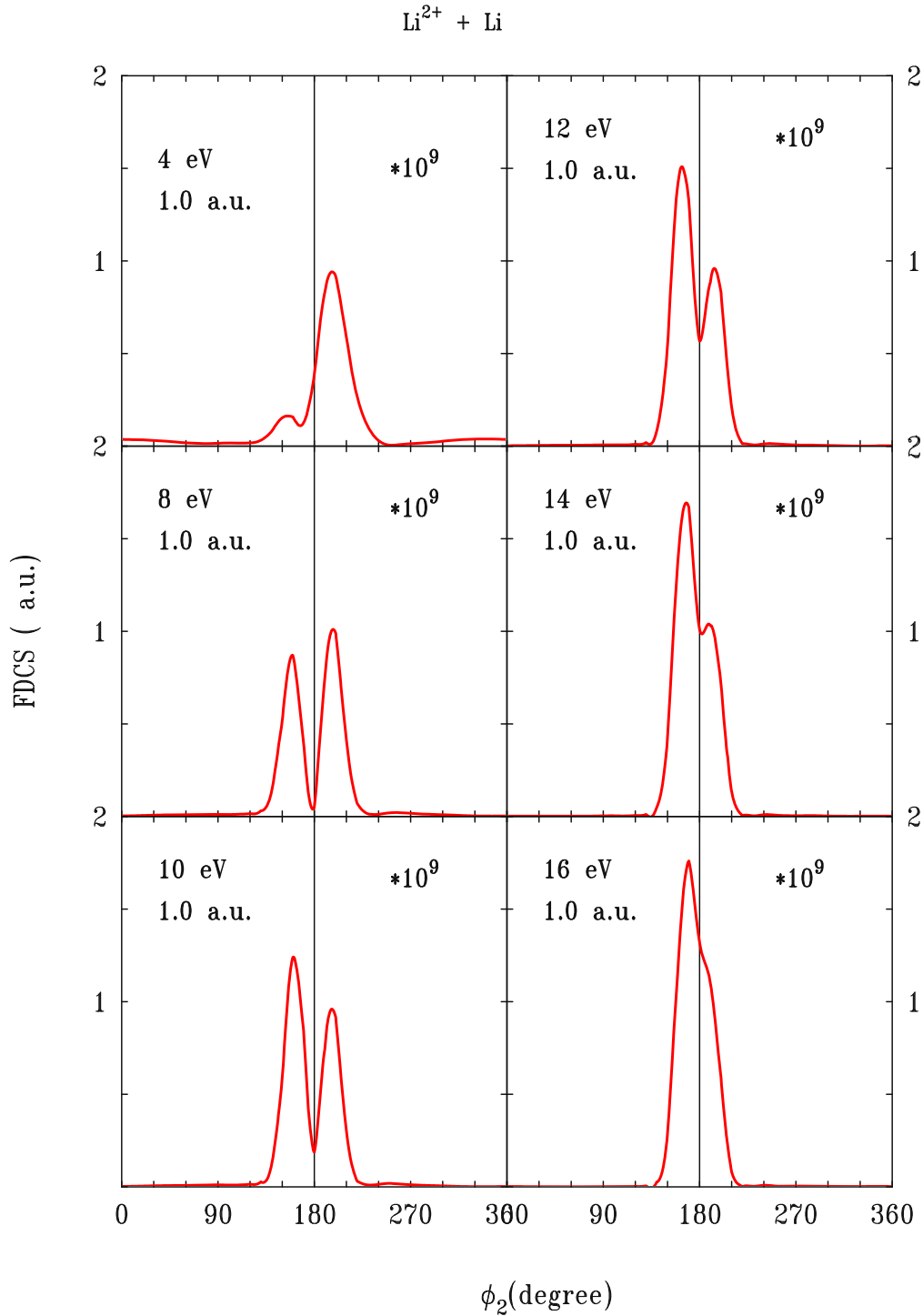


Figure 8. Fully differential cross sections for 16 MeV Li^{2+} ionization of the $2p$ shell of Li [86% ($m = -1$), 9% ($m = 0$), 5% ($m = +1$)] in the azimuthal plane as a function of the azimuthal angle for a range of ejected electron energies between 4 and 16 eV. The energy of the ejected electron in eV, the momentum transfer of the projectile in atomic units (a.u.), and the magnitude of the cross section in atomic units (a.u.) is noted in each panel.

Otranto and Olson [58] examined the development of the double peak for 200 eV electron and positron impact ionization of argon as a function of momentum transfer and found double peaks occurring for increasing momentum transfer. They attributed this to the increasing dominance of the $m = 0$ contribution. However, for our case, the $m = 0$ contribution is insignificant and the double peak results entirely from the

$m = -1$ contribution. Figure 8 shows the theoretical FDCS for a fixed momentum transfer of $q = 1.0$ a.u. and a range of ejected electron energies between 4 and 16 eV. From the figure, it is seen that a very small shoulder at 4 eV for angles less than 180° develops into a peak of equal size as the peak for angles larger than 180° by 8 eV. For energies above 10 eV, the small angle peak increases in size and the large

angle peak reduces to a shoulder by 16 eV and then is completely gone by 20 eV. Consequently, it is clear that the double peak structure is determined by the angular part of the wavefunction and the kinematics but not the interactions. It would be very interesting to see if an experiment with better resolution would confirm the existence of this double binary peak structure.

5. Conclusions

We report here the first experimental FDCS measurements for single ionization of the $2s$ and $2p$ states of Li in the azimuthal plane by ion impact in the perturbative regime. Three different ejected electron energies (2, 10 and 20 eV) were measured and, for each energy, two different momentum transfers.

We compared the experimental results with theoretical 3DW-EIS FDCS and found reasonably good agreement with experiment. Theory gave very good agreement with the shape and peak positions of the experimental data and not so good agreement with the relative magnitudes. Theory predicted a double binary peak structure for $E_e = 10$ eV and $q = 1.0$ a.u. which could not be resolved with the current experimental resolution. Electron-impact FDCS were known to sometimes find a double binary peak structure and sometimes a single peak for ionization of p -states and the current theoretical results exhibited the same behavior. Since the 3DW-EIS results were in very good agreement with the shape of the other measured cases, it seemed reasonable to expect that the predicted double peak structure was correct. Consequently, we performed a series of calculations to see what caused the double peak and how to predict when one should expect to find a double peak. We first determined that the double peak was caused by the angular part of the p -state wavefunction. Next, we tried to determine which forces could cause the peak to appear by performing calculations with different interactions either turned on or off.

We found that the projectile nucleus-target ion interaction only had a noticeable effect on the shape of the smallest cross sections and otherwise it was not very important for the kinematics examined here. We also examined the importance of the ejected electron interactions with the final state ion and discovered that short range screening of the nucleus was not very important. However, it was important to include the long range Coulomb interaction. None of these interactions had an effect on the double peak structure. Consequently, we learned that the angular part of the p -state wavefunction caused the double peaks but none of the interactions in the calculation seemed to have an impact on the double peak.

We then performed a series of calculations for a fixed ejected electron energy of 10 eV and different momentum transfers and found that the double peaks occur for a small range of momentum transfers between $q = 0.9$ a.u. and $q = 1.2$ a.u. We also performed a series of calculations for $q = 1.0$ a.u. and different ejected electron energies and found that a small angle shoulder develops into a peak between 4 and 8 eV and that the high angle peak reduces to a shoulder

between 10 and 16 eV. Since changing the kinematics caused the double peaks to disappear but varying the forces did not, it is clear that the double peaks are caused by the angular part of the p -state wavefunction and the kinematics only. What is not clear is how to predict the kinematical conditions which produce the double peak. Finally we would note that the present Li^{2+} and previously measured O^{8+} [43] results were very different for the $2s$ state. We think the reason is that, for the higher projectile mass and charge, small impact parameters are more important which means that the cross sections will be more sensitive to the nodal structure of the target.

Acknowledgments

DM and MS would like to acknowledge the support of the US National Science Foundation under Grant Nos PHY-1505819, PHY-1401586 and PHY-1703109, respectively. EGA would like to acknowledge sabbatical support provided by Missouri S&T and the University of Isfahan. DF was supported by an Emmi Noether grant from the German Research Foundation under grant No. FI 1593/1-1.

ORCID iDs

Ebrahim Ghanbari-Adivi  <https://orcid.org/0000-0003-3844-0928>

Daniel Fischer  <https://orcid.org/0000-0003-3870-9843>

References

- [1] Schulz M, Moshhammer R, Fischer D, Kollmus H, Madison D H, Jones S and Ullrich J 2003 *Nature* **422** 48
- [2] Rescigno T, Baertschy M, Isaacs W A and McCurdy C E 1999 *Science* **286** 2474
- [3] Lahmam-Bennani A 1991 *J. Phys. B: At. Mol. Opt. Phys.* **24** 2401
- [4] Rosel T, Röder J, Frost L, Jung K, Ehrhardt H, Jones S and Madison D H 1992 *Phys. Rev. A* **46** 2539
- [5] Dürr M, Dimopoulou C, Najjari B, Dorn A, Bray I, Fursa D V, Chen Z J, Madison D H, Bartschat K and Ullrich J 2006 *J. Phys. B: At. Mol. Opt. Phys.* **39** 4097
- [6] Jones S and Madison D H 2000 *Phys. Rev. A* **62** 042701
- [7] Colgan J, Pindzola M S, Robicheaux F J, Griffin D C and Baertschy M 2002 *Phys. Rev. A* **65** 042721
- [8] Bartlett P L and Stelbovics A T 2004 *Phys. Rev. Lett.* **93** 233201
- [9] Ehrhardt H, Schulz M, Tekaas T and Willmann K 1969 *Phys. Rev. Lett.* **22** 89
- [10] Ullrich J, Moshhammer R, Dorn A, Dörner R, Schmidt L and Schmidt-Böcking H 2003 *Rep. Prog. Phys.* **66** 1463
- [11] Dörner R, Mergel V, Jagutzki O, Spielberger L, Ullrich J, Moshhammer R and Schmidt-Böcking H 2000 *Phys. Rep.* **330** 192
- [12] Schulz M, Moshhammer R, Perumal A N and Ullrich J 2002 *J. Phys. B: At. Mol. Opt. Phys.* **35** L161
- [13] Schulz M, Moshhammer R, Fischer D and Ullrich J 2003 *J. Phys. B: At. Mol. Opt. Phys.* **36** L311

- [14] Voitkiv A B, Najjari B, Moshhammer R, Schulz M and Ullrich J 2004 *J. Phys. B: At. Mol. Opt. Phys.* **37** L365
- [15] Hubele R et al 2013 *Phys. Rev. Lett.* **110** 133201
- [16] Gassert H et al 2016 *Phys. Rev. Lett.* **116** 073201
- [17] Schulz M and Madison D H 2006 *Int. J. Mod. Phys. A* **21** 3649
- [18] Maydanyuk N V, Hasan A, Foster M, Tooke B, Nanni E, Madison D H and Schulz M 2005 *Phys. Rev. Lett.* **94** 243201
- [19] Hasan A et al 2016 *J. Phys. B: At. Mol. Opt. Phys.* **49** 04LT01
- [20] Sharma S, Arthanayaka T P, Hasan A, Lamichhane B R, Remolina J, Smith A and Schulz M 2014 *Phys. Rev. A* **89** 052703
- [21] Sharma S, Arthanayaka T P, Hasan A, Lamichhane B R, Remolina J, Smith A and Schulz M 2014 *Phys. Rev. A* **90** 052710
- [22] Arthanayaka T P, Sharma S, Lamichhane B R, Hasan A, Remolina J, Gurung S and Schulz M 2015 *J. Phys. B: At. Mol. Opt. Phys.* **48** 071001
- [23] Arthanayaka T, Lamichhane B R, Hasan A, Gurung S, Remolina J, Borbély S, Járαι-Szabó F, Nagy L and Schulz M 2016 *J. Phys. B: At. Mol. Opt. Phys.* **49** 13LT02
- [24] Wang X, Schneider K, LaForge A, Kelkar A, Grieser M, Moshhammer R, Ullrich J, Schulz M and Fischer D 2012 *J. Phys. B: At. Mol. Opt. Phys.* **45** 211001
- [25] Fischer D et al 2012 *Phys. Rev. Lett.* **109** 113202
- [26] Hubele R et al 2015 *Rev. Sci. Instrum.* **86** 033105
- [27] LaForge A C et al 2013 *J. Phys. B: At. Mol. Opt. Phys.* **46** 031001
- [28] Crothers D S F 1982 *J. Phys. B: At. Mol. Opt. Phys.* **15** 2061
- [29] Crothers D S F and McCann J F 1983 *J. Phys. B: At. Mol. Opt. Phys.* **16** 3229
- [30] Salin A 1989 *J. Phys. B: At. Mol. Opt. Phys.* **22** 3901
- [31] Fainstein P D, Ponce V H and Rivarola R D 1991 *J. Phys. B: At. Mol. Opt. Phys.* **24** 3091
- [32] Fainstein P D, Gulyás L and Salin A 1994 *J. Phys. B: At. Mol. Opt. Phys.* **27** L259
- [33] Gulyás L, Fainstein P D and Salin A 1995 *J. Phys. B: At. Mol. Opt. Phys.* **28** 245
- [34] Rodríguez V D and Barrachina R O 1998 *Phys. Rev. A* **57** 215
- [35] Gulyás L and Fainstein P D 1998 *J. Phys. B: At. Mol. Opt. Phys.* **31** 3297
- [36] Fiol J, Rodríguez V D and Barrachina R O 2001 *J. Phys. B: At. Mol. Opt. Phys.* **34** 933
- [37] Belkić D 2003 *Principles of Quantum Scattering Theory* (Bristol: Institute of Physics Publishing)
- [38] Voitkiv A B, Najjari B and Ullrich J 2003 *J. Phys. B: At. Mol. Opt. Phys.* **36** 2591
- [39] Ciappina M F and Cravero W R 2006 *J. Phys. B: At. Mol. Opt. Phys.* **39** 2183
- [40] Belkić D 2008 *Quantum Theory of High-Energy Ion-Atom Collisions* (London: Taylor and Francis)
- [41] Belkić D, Mancev I and Hanssen J 2008 *Rev. Mod. Phys.* **80** 249
- [42] Gulyás L, Egri S and Kirchner T 2014 *Phys. Rev. A* **90** 062710
- [43] Ghanbari-Adivi E, Fischer D, Ferreira N, Goullon J, Hubele R, LaForge A, Schulz M and Madison D 2016 *Phys. Rev. A* **94** 022715
- [44] Gell-Mann M and Goldberger M L 1953 *Phys. Rev.* **91** 398
- [45] Madison D H, Fischer D, Foster M, Schulz M, Moshhammer R, Jones S and Ullrich J 2003 *Phys. Rev. Lett.* **91** 253201
- [46] Green A E S, Sellin D L and Zachor A S 1969 *Phys. Rev.* **184** 1
- [47] Szydlik P P and Green A E S 1974 *Phys. Rev. A* **9** 1885
- [48] Garvey R H, Jackman C H and Green A E S 1975 *Phys. Rev. A* **12** 1144
- [49] Jones S and Madison D H 1998 *Phys. Rev. Lett.* **81** 2886
- [50] Stevenson M A, Hargreaves L R, Lohmann B, Bray I, Fursa D V, Bartschat K and Kheifets A 2009 *Phys. Rev. A* **79** 012709
- [51] Hargreaves L R, Stevenson M A and Lohmann B 2010 *J. Phys. B: At. Mol. Opt. Phys.* **43** 205202
- [52] Haynes M A and Lohmann B 2001 *Phys. Rev. A* **64** 044701
- [53] Stevenson M A and Lohmann B 2008 *Phys. Rev. A* **77** 032708
- [54] Ren X, Amami S, Zatsarinny O, Pflüger T, Weyland M, Dorn A, Madison D and Bartschat K 2016 *Phys. Rev. A* **93** 062704
- [55] Ozer Z N et al 2016 *Phys. Rev. A* **93** 062707
- [56] Whelan C T 2013 *Fragmentation Processes: Topics in Atomic and Molecular Physics* ed C T Whelan (Cambridge: Cambridge University Press) pp 223–60
- [57] McGovern M, Assafrao D, Mohallem J R, Whelan C T and Walters H R J 2010 *Phys. Rev. A* **81** 042704
- [58] Otranto S and Olson R E 2009 *Phys. Rev. A* **80** 012714